Fano-Doppler Laser Cooling of Hybrid Nanostructures

Alessandro Ridolfo,[†,‡] Rosalba Saija,[‡] Salvatore Savasta,[‡] Philip H. Jones,[§] Maria Antonia Iatì,[†] and Onofrio M. Maragò[†,*]

[†]Istituto per i Processi Chimico-Fisici, IPCF-CNR, I-98158 Messina, Italy, [‡]Dipartimento di Fisica della Materia e Ingegneria Elettronica, Universitá di Messina, Messina, Italy, and [§]Department of Physics and Astronomy, University College London, WC1E 6BT London, United Kingdom

ABSTRACT Laser cooling the center-of-mass motion of systems that exhibit Fano resonances is discussed. We find that cooling occurs for red or blue detuning of the laser frequency from resonance depending on the Fano factor associated with the resonance. The combination of the Doppler effect with the radiation cross-section quenching typical of quantum interference yields temperatures below the conventional Doppler limit. This scheme opens perspectives for controlling the motion of mesoscopic systems such as hybrid nanostructures at the quantum regime and the exploration of motional nonclassical states at the nanoscale.

KEYWORDS: Fano resonances · laser cooling · hybrid nanostructures · electromagnetic scattering theory

In the last decades, laser cooling[1−4] has been at the heart of intense research in atomic physics.[5] The ability to precisely control the external degrees of freedom, such as position and momentum, of atomic systems has led to outstanding achievements such as Bose−Einstein condensation of alkali metal atoms,[6,7] investigation of many-body physics with ultracold gases,[8] and ion[9] and molecule[10] cooling for quantum information processing.[11,12] Moreover, optical forces are the crucial enabling step in experiments and protocols aimed at probing the quantum regime of complex particles,[13,14] emerging quantum phenomena at the macroscale,[15,16] and opto-mechanics.[17] Despite this great success, extending conventional laser cooling to anything beyond an alkali-like atomic species is challenging.

Quantum interference is ubiquitous in physics.[18,19] It is often evidence of the emerging quantum nature of a system. Historically, the interference between two transition amplitudes was independently pioneered by Majorana[20,21] and Fano[22,23] in the context of autoionization.[18] Quantum interference between discrete energy levels[24,25] also plays a special role in laser cooling of atoms where the occurrence of coherent states uncoupled with the light is responsible for sub-recoil[4] and electromagnetic-induced transparency-assisted cooling.[26−28] The so-called Fano line shapes have now been shown to occur in a huge variety of systems,[19,29−32] as a consequence of the coupling of a system with a discrete energy spectrum to a continuum or quasi-continuum of states. Of particular interest are hybrid nanostructures, that is, systems composed of a quantum emitter (QE) and a plasmonic nanoparticle, which have very recently been shown to exhibit both extinction and scattering cross sections with Fano resonance line shapes[32−36] as the discrete levels of the QE are coupled to the plasmonic quasi-continuum.

Here we show how the variation of radiation pressure cross section around a Fano resonance can lead to a velocity-dependent scattering force and hence optical cooling. Surprisingly, this scheme which relies on the Doppler effect is capable of producing cooling below the conventional Doppler cooling limit because of the unique features of the Fano resonance line shape. We first describe a general analysis of laser cooling on systems with scattering and absorption cross sections exhibiting a Fano line shape and identify a nonlinear cooling regime when the laser wavelength is tuned in the vicinity of the destructive interference region. Then we focus on how this scheme can be applied to hybrid nanostructures and estimate the ultimate temperature in the milli-Kelvin range for exemplar structures consisting of a quantum dot (QD) coupled to a silver nanoparticle or dimer.

RESULTS AND DISCUSSION

Laser Cooling on a Fano Line Shape. We start by considering the scattering force on a particle at rest[5,37] (see also Methods):

$$F_{\mathrm{rad}} = \frac{nI}{c} C_{\mathrm{rad}} \qquad (1)$$

where n is the refractive index of the surrounding medium that in the following is assumed to be vacuum ($n = 1$), I the light

* Address correspondence to marago@me.cnr.it.

Received for review June 17, 2011 and accepted August 1, 2011.

Published online August 01, 2011
10.1021/nn2022364

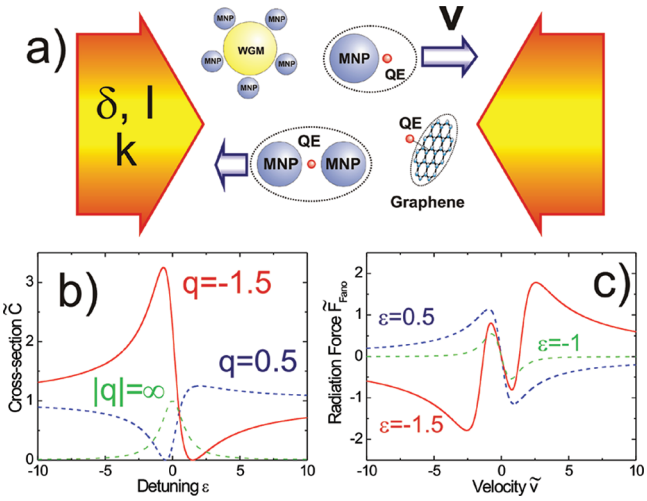

Figure 1. (a) Sketch illustrating the laser cooling configuration for a number of hybrid nanostructures. Two counter-propagating laser beams interact with hybrid metal (MNP)−quantum emitter (QE) nanoparticles, silica microparticles sustaining whispering gallery modes (WGM) hybridized with plasmonic nanoparticles, graphene flakes hybridized with a QE. The near-resonant excitation close to a Fano resonance is tuned by changing the incident light parameters (δ,I) as well as the coupling within the hybrid system (q,Γ) (see also refs 32−35). Radiation pressure cross section $\tilde{C}(\varepsilon)$ (b) and Fano cooling force, $\tilde{F}_{\mathrm{Fano}}(\tilde{v})$ (c). The Fano line shape and Fano factor, q, change with the coupling within the hybrid particle. The plots for a Lorentzian, $|q| = \infty$ (green dashed), and two Fano line shapes, $q = 0.5$ (blue dashed) and $q = -1.5$ (red solid), are shown. In the region around $\tilde{v} = 0$, the force has a linear dependence demonstrating velocity damping for all three line shapes.

intensity, c the velocity of light, and C_{rad} the radiation pressure cross section. The latter can be expressed (see Methods) in terms of the extinction and scattering cross sections as[37−39] $C_{\mathrm{rad}} = C_{\mathrm{ext}} - gC_{\mathrm{sc}}$, where g is the asymmetry parameter that depends on the shape and optical properties of the particle ($g = 0$ for a Rayleigh scatterer). For systems exhibiting sharp optical resonances, for example, atoms, molecules, quantum emitters, or systems with whispering gallery modes, both C_{ext} and C_{sc} exhibit a Lorentzian line shape that determines the behavior of near-resonance optical forces.[5] Now consider a system with a radiation pressure cross section exhibiting a Fano line shape resonance such as the hybrid nanostructures discussed above. In this case

$$C_{\mathrm{rad}} = C_{\mathrm{a}}\frac{\left(q\frac{\Gamma}{2}+\omega-\omega_0\right)^2}{(\omega-\omega_0)^2+\frac{\Gamma^2}{4}}+C_{\mathrm{b}} \qquad (2)$$

where q is the Fano factor, which characterizes the interference of amplitudes for transitions involving the discrete and continuum states[18,19,29] (q regulates the line profile that for $|q| \to \infty$ it becomes Lorentzian), Γ is the full width half-maximum (FWHM), ω_0 is the Fano resonance frequency, and C_{a} and C_{b} are the amplitudes of the resonant and background cross sections, respectively.

We now consider a particle with mass m moving in one dimension at velocity v under the influence of two counter-propagating laser beams (1D optical molasses[5]) with wavevector k, and detuned from the Fano resonance by an amount $\delta = \omega - \omega_0$ (see Figure 1a for a sketch). This results in Doppler shifts of $\mp kv$ from the stationary particle resonance peak and thus a net radiation force acting on the particle of $F_{\mathrm{Fano}} = (I/c)(C^{+}_{\mathrm{rad}} - C^{-}_{\mathrm{rad}})$, where the $+$ and $-$ denote the cross sections for the wavevectors parallel and antiparallel to the velocity:

$$C^{\pm}_{\mathrm{rad}} = C_{\mathrm{a}}\frac{\left(q\frac{\Gamma}{2}+\delta\mp kv\right)^2}{(\delta\mp kv)^2+\frac{\Gamma^2}{4}}+C_{\mathrm{b}} \qquad (3)$$

In order to examine the general features of the Fano radiation force and cooling process, it is useful to define the reduced (dimensionless) quantities $\tilde{C} = (C_{\mathrm{rad}} - C_{\mathrm{b}})/C_{\mathrm{a}}$, $\varepsilon = 2\delta/\Gamma$, and $\tilde{v} = v/v_{\mathrm{c}}$, where $v_{\mathrm{c}} = \Gamma/2k$ is the velocity capture range of the cooling process defining the range in which the force is linear with velocity (see Figure 1c). Thus the reduced Fano radiation cross section is (Figure 1b) $\tilde{C} = (q + \varepsilon)^2/(\varepsilon^2 + 1)$, which yields a reduced Fano radiation force (Figure 1c):

$$\tilde{F}_{\mathrm{Fano}} = \frac{cF_{\mathrm{Fano}}}{IC_{\mathrm{a}}} = \frac{(q+\varepsilon-\tilde{v})^2}{(\varepsilon-\tilde{v})^2+1} - \frac{(q+\varepsilon+\tilde{v})^2}{(\varepsilon+\tilde{v})^2+1} \qquad (4)$$

For small velocities ($\tilde{v} \ll 1$), the force can be linearized in $\tilde{v}$, $\tilde{F}_{\mathrm{Fano}} \approx -\tilde{\alpha}(q,\varepsilon)\tilde{v}$, with

$$\tilde{\alpha} = \frac{4(q+\varepsilon)}{\varepsilon^2+1}\left[1-\frac{\varepsilon(q+\varepsilon)}{(\varepsilon^2+1)}\right] \qquad (5)$$

being the damping coefficient of the process. Cooling of the center-of-mass motion of the particle occurs when $\tilde{\alpha} > 0$, while heating occurs for $\tilde{\alpha} < 0$. In comparison with conventional Doppler cooling on a Lorentzian line shape resonance, we now have an additional

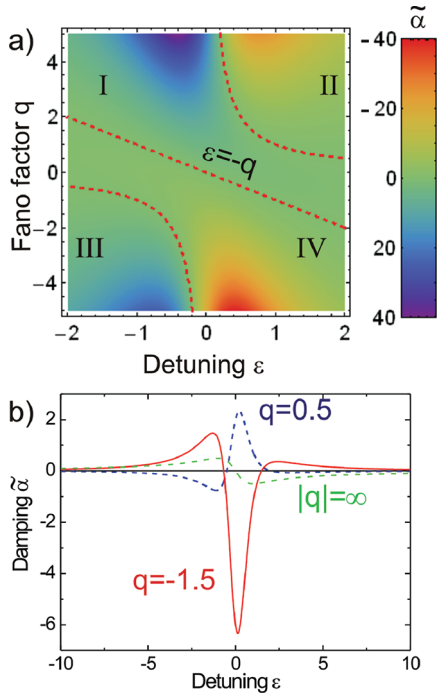

Figure 2. (a) Density plot of damping $\tilde{\alpha}$: in the regions I and III, we have cooling; on the contrary, in the regions II and IV, laser heats specimen with the same Doppler mechanism. The red dashed line represents the locus of points where $\tilde{\alpha} = 0$. (b) Damping $\tilde{\alpha}$ as a function of detuning for the standard Lorentzian case, $|q| = \infty$ (green dashed), and two Fano factors $q = 0.5$ (blue dashed) and $q = -1.5$ (red solid). For positive damping, the particles are cooled, while negative damping is associated with heating.

dependence of the damping coefficient on the Fano (line shape) factor, q. Figure 2a shows an intensity plot of the damping coefficient as a function of the Fano factor and detuning. Four regions can be identified corresponding to either cooling, regions I and III, or heating, regions II and IV. The light-particle interaction in II and III presents similarities with the standard cooling/heating process on a Lorentzian line shape; for example, cooling occurs for red detuning, while heating occurs for blue detuning. However, in regions I and IV, the quantum interference giving rise to the Fano profile is responsible for unconventional Doppler cooling/heating. Not only can the cooling/heating processes occur for blue/red detuning (conversely to the Lorentzian case) but also the line defined by $\varepsilon = -q$ is a *dark* line where damping and reduced radiation cross section vanish. Examples of damping curves that illustrate the occurrence of heating and cooling at detunings where a Lorentzian line shape would experience the opposite effect are shown in Figure 2b for values of the Fano factor $q = 0.5$ and -1.5. Thus, while for a Lorentzian line shape there is a maximum for $\varepsilon = -1$,[5] for a Fano line shape, the detuning corresponding to the maximum damping is dependent on q.

We now focus on parameters (ε,q) in regions I and III where cooling occurs and calculate the cooling temperature as a balance between the cooling process that damps the average energy of the particle in a characteristic time $\tau = m/2\alpha$ and the heating by the random momentum diffusion due to photon scattering with rate $R(\varepsilon,q) = F_{rad}/\hbar k$.[5] The balance between these two competing processes yields the equilibrium temperature that for laser cooling in 1D is written as[5] $k_B T = (1 + \eta)\hbar^2 k^2 R/\alpha$. Here η is a geometrical factor that takes into account the angular averaged redistribution of scattered photons and for a Rayleigh particle (isotropic scattering) is[5] $\eta = 1/3$. For a particle with a Lorentzian resonance of width Γ, this yields the standard Doppler limit temperature of $k_B T_D = (1 + \eta)\hbar\Gamma/4 = \hbar\Gamma/3$. Thus, following the same analysis and using eqs 1, 2, and 5 for the Fano-Doppler cooling process we find that

$$\frac{T_F}{T_D} = \frac{2}{\tilde{\alpha}}\left(\tilde{C} + \frac{C_b}{C_a}\right) \tag{6}$$

We first consider the case with no background contribution to the radiation cross section ($C_b = 0$) for which

$$\frac{T_F}{T_D} = \frac{(q+\varepsilon)(\varepsilon^2+1)}{2(1-\varepsilon q)} \tag{7}$$

Figure 3a shows an intensity plot of the Fano-Doppler equilibrium temperature as a function of detuning and Fano factor. In region III, the cooling process is similar to conventional Doppler cooling and occurs for red detuning and negative Fano factors. The minimum temperature in region III is always larger than T_D and depends on the specific value of q. In region I, however, due to the quantum interference phenomena that determine the Fano line shape and scattering cross section, as $\varepsilon \to -q$ sub-Doppler temperatures can be achieved. In the proximity of the dark line, $\varepsilon = -q$, the temperature of the process tends asymptotically (in an infinite time) to zero, but in this proximity, the linear Doppler theory cannot be applied. In fact, when $\varepsilon \approx -q$ and $\tilde{v} \ll q$, the force in eq 4 is nonlinear with velocity, $\tilde{F}_{Fano} \approx -4q\tilde{v}^3/(q^2+1)^2$. Thus the corresponding damping, $\tilde{\alpha}(q,\tilde{v}) \approx 4q\tilde{v}^2/(q^2+1)^2$, yields an asymptotic nonlinear diffusion toward zero momentum. More generally, close to the dark line where low temperatures are achieved, the cooling process is non-ergodic and a sub-recoil theory should be used.[4] This is particularly important when a narrow line width atomic or molecular system is coupled to a plasmonic landscape (*e.g.*, such as occurs in the case of doped graphene[35]).

We now consider a small background in the radiation cross section, $C_b \neq 0$. Far from the dark line, the effect of a small background on the cooling process and equilibrium temperature is negligible because of the counter-propagating configuration. However, close to the dark line, the cooling process is now regulated by the background rate $R_b = IC_b/\hbar\omega$. In particular, the equilibrium temperature is related to the second term in eq 6, $T_F/T_D \approx 2C_b/\tilde{\alpha}C_a$, while the

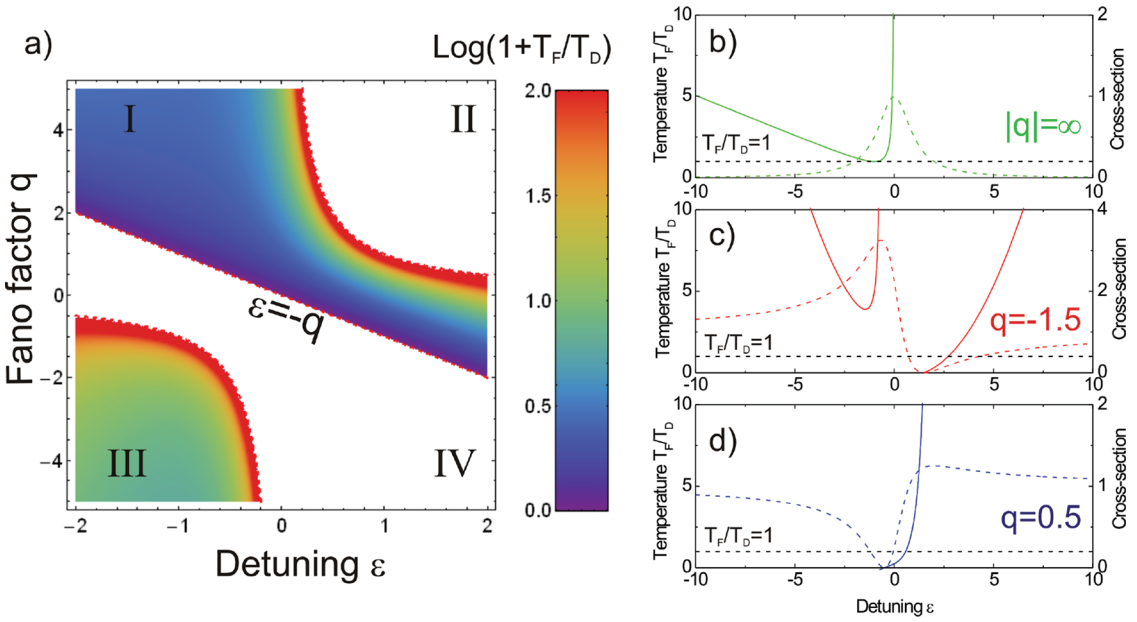

Figure 3. Density plot of the equilibrium temperature, $T_F(q,\varepsilon)$, achieved by the Fano cooling process normalized to the conventional Doppler limit, T_D. Fano cooling resembles standard Doppler cooling in region III, while sub-Doppler temperatures are achieved in region I. In the proximity of $\varepsilon = -q$, the temperature goes asymptotically to zero, but linear Doppler theory fails. (b) Temperature plot for standard Doppler cooling (green solid line) on a Lorentzian line shape (green dashed line), $|q| = \infty$. The minimum temperature is T_D, obtained for $\varepsilon = -1$ (black dashed). (c) Fano cooling temperature (red solid) on a line shape with $q = -1.5$ (red dashed). The left branch corresponds to region III and occurs only for red detuning. The right branch corresponds to region I. Sub-Doppler temperatures are achieved when approaching $\varepsilon \approx 1.5$. In (d), we show the temperature (blue solid) for $q = 0.5$ (blue dashed). Here there is no left branch, while only the right branch corresponding to region I is present. Sub-Doppler temperature are achieved close to $\varepsilon \approx -0.5$.

nonlinear force leads to an anomalous diffusion regime at small momenta. Note that if the ergodic time scale, R_b^{-1}, is much larger than a microscopic time scale for non-ergodic diffusion, $\tau_0 = \hbar\omega(q^2 + 1)/IC_a$, a sub-recoil regime is reached.[4] The fractional change of the momentum distribution width in this regime can be estimated following sub-recoil laser cooling theory as[4] $\delta\tilde{p} \approx ((q^2 + 1)C_b/C_a)^{1/2}$.

Hybrid Nanostructures. We now focus on the Fano cooling of hybrid nanostructures composed of a QD coupled to a single silver nanoparticle (Figure 4a) or to a silver nanoparticle dimer (Figure 4b). In these systems, the position and shape of the Fano resonances can be varied by changing the interparticle distance and the detuning Δ between the QD and the surface plasmon mode resonances, thus different Fano factors q can be engineered. In the first case, we consider a silver nanosphere with radius r = 8 nm, whose frequency-dependent dielectric permittivity is gathered interpolating the experimental data of Johnson and Christy,[40] and a QD with dipole moment μ/e = 0.7 nm. The distance between the centers of the two nanoparticles is 14 nm. The QD excitonic resonance is detuned by Δ = 60 meV from the plasmon resonance peak (see insets in Figure 4). The radiative cross sections C_{rad} displayed in Figure 4 are calculated through electromagnetic scattering theory in the transition matrix formalism[34] (see Methods). We consider a spherical QD with radius r_{QD} = 2 nm. Because of its symmetry, a spherical QD has three energy-degenerate bright excitons with optical dipoles parallel to the three direction x, y, and z. Hence, the QD can be described in its simplest way as an isotropic effective medium with a single resonance at the energy $\hbar\omega_0$ of the lowest energy exciton. The resulting frequency dependent permittivity can be expressed as[34]

$$\varepsilon_r(\omega) = \varepsilon_b + \frac{A}{\omega_0^2 - \omega^2 - 2i\omega\gamma_0} \qquad (8)$$

where γ_0 is the total broadening of the excitonic resonance, ε_b describes the background dielectric constant, and $A = \mu^2/(\varepsilon_0 V)$, with μ being the dipole moment and V the dot volume. In both cases, the hybrid nanostructures are embedded in a dielectric shell (*e.g.*, a polymer) with refractive index[33,34] $n_{shell} = \sqrt{\varepsilon_b} = 1.7$ in order to bind the QD and MNP and fix their distance in a core−shell structure. In the second case, we employ a QD (μ/e = 0.3 nm) in the center (*hot spot*[41]) of a pair of silver spheres of radius r = 8 nm separated by a gap of 8 nm with Δ = 60 meV. The strong field enhancement in the dimer gap enables strong Fano effects even for QDs with small dipole moments.

For a laser power of 10 mW focused on a spot size of 100 μm, we obtain cooling times below 5 s. However, the heating due to the nonradiative background, C_b, limits the temperature to about half of the Doppler limit, that is, $T \approx 1.7$ K (corresponding to a root-mean-square velocity $v_{rms} \approx 40$ mm/s) for the single sphere

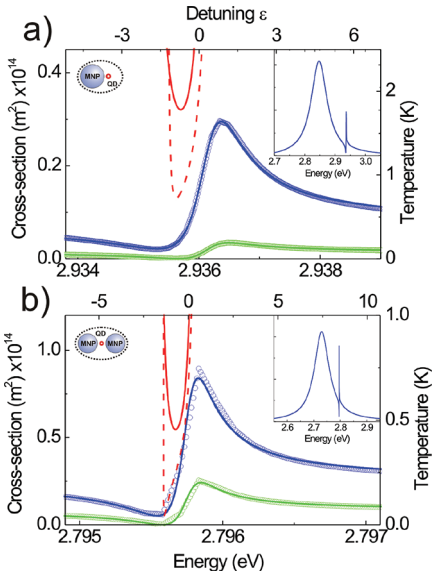

Figure 4. Radiation pressure (blue) and scattering (green) cross sections for hybrid nanostructures composed of (a) a QD coupled to a single silver nanoparticle and (b) a QD in the *hot spot* of a silver nanoparticle dimer. Insets show the full radiation cross-section curves with the broad plasmon resonance from the silver nanoparticles. From the fit (blue and green lines) of the narrow profiles with a Fano line shape, we get Fano factors $q = 1.99$ for the single sphere (a) and $q = 1.71$ for the dimer. The equilibrium temperature of the Fano cooling is plotted with a red dashed line when considering only the radiative processes (scattering) and with a solid red line when considering also the nonradiative background. By tuning the laser to $\varepsilon \approx -0.71$, we estimate temperatures of about 1.7 K for the single sphere and 450 mK for the dimer when considering the nonradiative background (red line). These correspond to velocities of 40 and 13 mm/s, respectively. When we consider only radiative process, we obtain equilibrium temperatures that are 670 mK for the single sphere and 45 mK for the dimer.

(Figure 4a) and $T \approx 450$ mK ($v_{rms} \approx 13$ mm/s) for the dimer (Figure 4b). On the other hand, when only the radiative processes are considered (Figure 4, green lines), temperatures 1 order of magnitude lower are achieved in few seconds (Figure 4, red dashed lines), 670 mK ($v_{rms} \approx 4$ mm/s) for the single sphere and 45 mK ($v_{rms} \approx 1.3$ mm/s) for the dimer. Nonradiative processes can be significantly reduced by employing smaller metal particles or nanoshells,[29,31,42] and therefore, the nonlinear regime could be reached.

Most of the ingredients needed for the application of this Fano-Doppler laser cooling scheme are within experimental reach with existing state-of-the-art technology. Nanostructures with Fano line shapes have already been produced using wet chemistry approaches.[29,31,42] Optical trapping[43] of nanoparticles (*e.g.*, graphene,[44] nanotubes,[45] quantum dots[46]) and nanoaggregates,[47] as well as ion trapping in vacuum of graphene,[48] has similarly been recently demonstrated. A possible experimental configuration would then involve different stages in a similar fashion as developed for the creation of ultracold atomic samples.[1−3,6,7] A spray of hybrid nanostructures dispersed in liquid environment could be used in vacuum,[48] the capture of few particles in a far-detuned (with infrared radiation) optical trap[44−47] or ion trap[48] can spatially limit and increase in time the interaction with light, thus a near-resonant radiation can be added to cool and detect the velocity distribution of nanoparticles as recently demonstrated at the microscale.[49]

As the application of laser cooling is in vacuum, it is now useful to discuss the role of the surrounding air molecules and compare the effect of the viscous damping during the cooling process of nanoparticles. For a particle trapped in a confining potential (*e.g.*, an optical trap or an ion trap) with harmonic frequency ω_t the dynamics of the center-of-mass motion can be described by a Langevin equation, that in one dimension is written as[14,15,51]

$$m\ddot{x}(t) = -m\omega_t^2 x(t) - (\alpha + \gamma)\dot{x} + f(t) \qquad (9)$$

where the total damping is now the sum of the viscous, γ, and laser cooling, α, damping coefficients and $f(t)$ is a stochastic uncorrelated force.[44,45,49] The viscous damping coefficient for a particle of radius r in the free molecular flow regime is[51,50] $\gamma = (4/3 + 3\pi/16)\pi\rho\bar{v}r^2$, where $\bar{v}$ is the root-mean-square velocity of air molecules ($\bar{v} \sim 500$ m/s at room temperature) and ρ is their density. Using the relation between density and pressure of a gas, $\rho = 3P/\bar{v}^2$, and considering the exemplar hybrid nanostructures discussed above, we thus obtain that $\gamma \sim 2 \times 10^{-20}P$[Torr] Ns/m. This is equal to the Fano optical damping, $\alpha \sim 2 \times 10^{-21}$ Ns/m (at $\varepsilon \approx -0.71$), of the dimer hybrid nanostructure at a pressure of about 0.1 Torr. The laser cooling damping is 5 orders of magnitude larger than that of the background gas at a pressure of $P \sim 10^{-6}$ Torr. Another effect of the residual gas is to increase the momentum fluctuations of the trapped particle motion through molecular collisions resulting in an increase in its final temperature. The recoil kick received by the particle during a collision with a gas molecule is about $\delta p_{coll} \sim 2.5 \times 10^{-23}$ kg m/s, while the collisional rate can be estimated as $R_{coll} \sim \pi r^2 P/\delta p_{coll} \sim 100\ s^{-1}$ at a pressure $P \sim 10^{-6}$ Torr. At this pressure, the diffusion in momentum space, $(\delta p_{coll})^2 R_{coll}$, due to collisions equals the diffusion due to photon recoil calculated for the dimer hybrid nanostructure, and the final temperature is 2 times larger than when considering the optical cooling only. However, at pressures of 10^{-8} Torr, easily achieved in a standard ultrahigh vacuum (UHV) chamber, the effect of background gas on the final temperature is 2 orders of magnitude smaller, ensuring optical cooling to be the only relevant process in reasonable UHV conditions.

CONCLUSIONS

In conclusion, we have shown how a system exhibiting a Fano line shape can be laser cooled below the

conventional Doppler cooling limit within a Doppler cooling scheme. The intrinsic quantum interference, *i.e.*, the hybridization of the quantum emitter with the larger particle providing the quasi-continuum of states, is responsible for the lower temperatures. Nonlinear laser cooling regimes are found when the laser wavelength is tuned close to the *dark* region of the extinction spectrum. Here the nonlinear diffusion in momentum space drives the particles toward zero momentum, while the equilibrium temperature is set by the background radiation cross section. We applied this model to hybrid nanostructures made of a quantum emitter and a plasmonic nanoparticle, estimating temperatures in the milli-Kelvin range for cooling times of few seconds that could be probed experimentally in combination with optical[44] or electric ion[48] traps. The scheme is general and can be applied to any large system hybridized with a quantum emitter exhibiting a Fano line shape, for example, a molecule coupled to a plasmonic landscape,[34] a bead with whispering gallery mode[51] hybridized with plasmonic particles, or a doped graphene flake.[35]

METHODS

Radiation Pressure Cross Section. The dynamical behavior of a particle under the effect of an electromagnetic field and other mechanical forces $\mathbf{F}_{mech}$, such as a trapping external force and resistance of the surrounding medium, is governed by the equation[37]

$$\frac{d}{dt}(\mathbf{P}_{mech} + \mathbf{P}_{field}) = \oint_S T_M \times \hat{\mathbf{n}} dS + \mathbf{F}_{mech} \quad (10)$$

where $\mathbf{P}_{mech}$ is the mechanical momentum of the particle and

$$\mathbf{P}_{field} = \frac{1}{4\pi c}\int_{\tilde{V}} (\mathbf{E} \times \mathbf{B})\, d\tilde{V} \quad (11)$$

is the momentum of the electromagnetic field. The integral in eq 11 is performed over the volume $\tilde{V}$, bounded by a regular surface S, of unit outward normal $\hat{\mathbf{n}}$, surrounding the particle. The integral on the right-hand side of eq 10 is the vector flux across the surface S of the Maxwell stress tensor

$$T_M = \frac{1}{4\pi}\left[\mathbf{E}\otimes\mathbf{E} + \mathbf{B}\otimes\mathbf{B} - \frac{1}{2}(\mathbf{E}\cdot\mathbf{E} + \mathbf{B}\cdot\mathbf{B})\mathrm{I}\right] \quad (12)$$

that represents the force that the electromagnetic field exerts on the particle. In eq 12, $\otimes$ denotes dyadic product and I is the unit dyad. Thus the time averaged radiation force on the particle is[52,53]

$$\mathbf{F}_{rad} = r^2 \int_\Omega \hat{\mathbf{r}} \langle T_M \rangle d\Omega \quad (13)$$

where the integration is over the full solid angle, r is the radius of the surface S surrounding the particle, and $\langle\rangle$ denotes time averaging.

Equations 10−12 are quite general and apply to particles of any shape for whatever form of the electromagnetic field. In the following, we assume that the particle under study is embedded into a homogeneous medium of (real) refractive index n, that the fields depend on time through the factor $\exp[-i\omega t]$ that is omitted throughout, and define the propagation constants *in vacuo* $k_v = \omega/c$ and in the surrounding medium $k = nk_v$. The field impinging on the particle is the polarized plane wave

$$\mathbf{E}_I = E_0 \hat{\mathbf{e}} \exp[i\mathbf{k}_I \cdot \mathbf{r}] \quad (14)$$

where $\hat{\mathbf{e}}$ is the (unit) polarization vector and $\mathbf{k}_I = k\hat{\mathbf{k}}_I$, while $\mathbf{E}_S$ denotes the field scattered by the particle. The surface S can be assumed to be a sphere whose center lies within the particle, with a unit outward normal $\hat{\mathbf{n}} = \hat{\mathbf{r}}$. The radius of the sphere is large enough that the scattered field can be evaluated in the far-field as

$$\mathbf{E}_S = E_0 \frac{e^{ikr}}{r} \mathbf{f}(\hat{\mathbf{k}}_S, \hat{\mathbf{k}}_I) \quad (15)$$

where $\mathbf{f}(\hat{\mathbf{k}}_S, \hat{\mathbf{k}}_I)$ is the scattering amplitude of the particle.[37,39]

We now define the differential scattering cross section:

$$\frac{dC_{sc}}{d\Omega} = |\mathbf{f}(\hat{\mathbf{k}}_S, \hat{\mathbf{k}}_I)|^2 \quad (16)$$

and by means of the optical theorem[37] for the extinction cross section

$$C_{ext} = \frac{4\pi}{k} \mathrm{Im}[\mathbf{f}(\hat{\mathbf{k}}_S = \hat{\mathbf{k}}_I, \hat{\mathbf{k}}_I) \cdot \hat{\mathbf{e}}^*] \quad (17)$$

it has been shown by Mishchenko[38] that the integral on the right-hand side of eq 10, that is, the radiation force, yields

$$\mathbf{F}_{rad} = \frac{I}{c}\left[C_{ext}\hat{\mathbf{k}}_I - \int_\Omega \frac{dC_{sc}}{d\Omega}\hat{\mathbf{k}}_S d\Omega\right] \quad (18)$$

where I is the incident intensity. Although the first term on the right-hand side of eq 18 is a force in the direction of the incident wave $\hat{\mathbf{k}}_I$, generally speaking, the direction of the total radiation force is different from the direction of propagation of the incident beam and depends on its polarization state, due to the second term in the equation.[54] In general, this should be taken into account when studying the dynamical behavior of a particle.[55] The projection of the force along $\hat{\mathbf{k}}_I$ turns out to be

$$F_{rad} = \mathbf{F}_{rad} \cdot \hat{\mathbf{k}}_I = \frac{I}{c}[C_{ext} - gC_{sc}] = \frac{I}{c}C_{rad} \quad (19)$$

where denoting by Φ the angle of scattering

$$g = \frac{1}{C_{sc}} \int \cos\Phi \frac{dC_{sc}}{d\Omega} d\Omega \quad (20)$$

is the asymmetry parameter.

Acknowledgment. We are grateful to E. Arimondo and F. Borghese for discussions, proof-reading, and support. M.A.I. and O.M.M. acknowledge support by FP7-HEALTH-F5-2009-241818-NANOANTENNA European project.

REFERENCES AND NOTES

1. Chu, S. The Manipulation of Neutral Particles. *Rev. Mod. Phys.* **1998**, *70*, 685–706.
2. Cohen-Tannoudji, C. Manipulating Atoms with Photons. *Rev. Mod. Phys.* **1998**, *70*, 707–719.
3. Phillips, W. D. Laser Cooling and Trapping of Neutral Atoms. *Rev. Mod. Phys.* **1998**, *70*, 721–740.
4. Bardou, F.; Bouchaud, J.-P.; Aspect, A.; Cohen-Tannoudji, C. *Lévy Statistics and Laser Cooling*; Cambridge University Press: Cambridge, 2002.
5. Foot, C. J. *Atomic Physics*; Oxford University Press: Oxford, 2005.
6. Cornell, E. A.; Wieman, C. E. Bose-Einstein Condensation in a Dilute Gas, the First 70 Years and Some Recent Experiments. *Rev. Mod. Phys.* **2002**, *74*, 875–893.

7. Ketterle, W. When Atoms Behave as Waves: Bose–Einstein Condensation and the Atom Laser. *Rev. Mod. Phys.* **2002**, *74*, 1131–1151.
8. Bloch, I.; Dalibard, J.; Zwerger, W. Many-Body Physics with Ultracold Gases. *Rev. Mod. Phys.* **2008**, *80*, 885–964.
9. Leibfried, D.; Blatt, R.; Monroe, C.; Wineland, D. Quantum Dynamics of Single Trapped Ions. *Rev. Mod. Phys.* **2003**, *75*, 281–324.
10. Ni, K.-K.; Ospelkaus, S.; de Miranda, M. H. G.; Peer, A.; Neyenhuis, B.; Zirbel, J. J.; Kotochigova, S.; Julienne, P. S.; Jin, D. S.; Ye, J. A High Phase-Space-Density Gas of Polar Molecules. *Science* **2008**, *322*, 231–235.
11. Zoller, P.; Beth, T.; Binosi, D.; Blatt, R.; Briegel, H.; Bruss, D.; Calarco, T.; Cirac, J. I.; Deutsch, D.; Eisert, J.; *et al.* Quantum Information Processing and Communication. *Eur. Phys. J. D* **2005**, *36*, 203–228.
12. DeMille, D. Quantum Computation with Trapped Polar Molecules. *Phys. Rev. Lett.* **2002**, *88*, 067901.
13. Gerlich, S.; Eibenberger, S.; Tomandl, M.; Nimmrichter, S.; Hornberger, K.; Fagan, P. J.; Tuxen, J.; Mayor, M.; Arndt, M.; *et al.* Quantum Interference of Large Organic Molecules. *Nat. Commun.* **2011**, *2*, 263.
14. Li, T.; Kheifets, S.; Raizen, M. G. Millikelvin Cooling of an Optically Trapped Microsphere in Vacuum. *Nat. Phys.* **2011**, *7*, 527–530.
15. Romero-Isart, O.; Juan, M. L.; Quidant, R.; Cirac, J. I. Toward Quantum Superposition of Living Organisms. *New J. Phys.* **2010**, *12*, 033015.
16. Romero-Isart, O.; Pflanzer, A. C.; Juan, M. L.; Quidant, R.; Kiesel, N.; Aspelmeyer, M.; Cirac, J. I. Optically Levitating Dielectrics in the Quantum Regime: Theory and Protocols. *Phys. Rev. A* **2011**, *83*, 013803.
17. Kleckner, D.; Bouwmeester, D. Sub-Kelvin Optical Cooling of a Micromechanical Resonator. *Nature* **2006**, *444*, 75–78.
18. Arimondo, E.; Clark, C. W.; Martin, W. C. Ettore Majorana and the Birth of Autoionization. *Rev. Mod. Phys.* **2010**, *82*, 1947–1958.
19. Miroshnichenko, A. E.; Flach, S.; Kivshar, Y. S. Fano Resonances in Nanoscale Structures. *Rev. Mod. Phys.* **2010**, *82*, 2257–2298.
20. Majorana, E. I Presunti Termini Anomali dell'Elio. *Nuovo Cimento* **1931**, *8*, 78–83.
21. Majorana, E. Teoria dei Tripletti *P′* Incompleti. *Nuovo Cimento* **1931**, *8*, 107–113.
22. Fano, U. Sullo Spettro di Assorbimento dei Gas Nobili presso il Limite dello Spettro d'Arco. *Nuovo Cimento* **1935**, *12*, 154–161; *J. Res. Natl. Inst. Stand. Technol.* **2005**, *110*, 583–590.
23. Fano, U. Effects of Configuration Interaction on Intensities and Phase Shifts. *Phys. Rev.* **1961**, *124*, 1866–1878.
24. Lounis, B.; Cohen-Tannoudji, C. Coherent Population Trapping and Fano Profiles. *J. Phys. II France* **1992**, *2*, 579–592.
25. Arimondo, E. Coherent Population Trapping in Laser Spectroscopy. In *Progress in Optics XXXV*; Wolf, E., Ed.; Elsevier: Amsterdam, 1996.
26. Morigi, G.; Eschner, J.; Keitel, C. H. Ground State Laser Cooling Using Electromagnetically Induced Transparency. *Phys. Rev. Lett.* **2000**, *85*, 4458–4461.
27. Morigi, G.; Arimondo, E. Two-Photon and Electromagnetically-Induced-Transparency-Assisted Doppler Cooling in a Three-Level Cascade System. *Phys. Rev. A* **2007**, *75*, 051404(R).
28. Dunn, J. W.; Thomsen, J. W.; Greene, C. H.; Cruz, F. C. Coherent Quantum Engineering of Free-Space Laser Cooling. *Phys. Rev. A* **2007**, *76*, 011401.
29. Lukyanchuk, B.; Zheludev, N. I.; Maier, S. A.; Halas, N. J.; Nordlander, P.; Giessen, H.; Chong, C. T. The Fano Resonance in Plasmonic Nanostructures and Metamaterials. *Nat. Mater.* **2010**, *9*, 707–715.
30. Fan, J. A.; Wu, C. H.; Bao, K.; Bao, J. M.; Bardhan, R.; Halas, N. J.; Manoharan, V. N.; Nordlander, P.; Shvets, G.; Capasso, F. Self-Assembled Plasmonic Nanoparticle Clusters. *Science* **2010**, *328*, 1135–1138.
31. Mukherjee, S.; Sobhani, H.; Lassiter, J. B.; Bardhan, R.; Nordlander, P.; Halas, N. J. Fanoshells: Nanoparticles with Built-in Fano Resonances. *Nano Lett.* **2010**, *10*, 2694–2701.
32. Zhang, W.; Govorov, A. O.; Bryant, G. W. Semiconductor–Metal Nanoparticle Molecules: Hybrid Excitons and Nonlinear Fano Effect. *Phys. Rev. Lett.* **2006**, *97*, 146804.
33. Ridolfo, A.; Di Stefano, O.; Fina, N.; Saija, R.; Savasta, S. Quantum Plasmonics with Quantum Dot–Metal Nanoparticle Molecules: Influence of the Fano Effect on Photon Statistics. *Phys. Rev. Lett.* **2010**, *105*, 263601.
34. Savasta, S.; Saija, R.; Ridolfo, A.; Di Stefano, O.; Denti, P.; Borghese, F. Nanopolaritons: Vacuum Rabi Splitting with a Single Quantum Dot in the Center of a Dimer Nanoantenna. *ACS Nano* **2010**, *4*, 6369–6376.
35. Koppens, F. H. L.; Chang, D. E.; Garcia de Abajo, F. J. Graphene Plasmonics: A Platform for Strong Light-Matter Interaction. **2011**, DOI: 10.1021/nl201771h.
36. Manjavacas, A.; Garcia de Abajo, F. J.; Nordlander, P. Quantum Plexcitonics: Strongly Interacting Plasmons and Excitons. *Nano Lett.* **2011**, *11*, 2318–2323.
37. Borghese, F.; Denti, P.; Saija, R. *Scattering from Model Nonspherical Particles*, 2nd ed.; Springer: Berlin, 2007.
38. Mishchenko, M. I. Radiation Force Caused by Scattering, Absorption, and Emission of Light by Nonspherical Particles. *J. Quant. Spectrosc. Radiat. Transfer* **2001**, *70*, 811–816.
39. Saija, R.; Iatì, M. A.; Giusto, A.; Borghese, F.; Denti, P.; Aiello, S.; Cecchi-Pestellini, C. Radiation Pressure Cross-Sections of Fluffy Interstellar Grains. *Mon. Not. R. Astron. Soc.* **2003**, *341*, 1239–1245.
40. Johnson, P. B.; Christy, R. W. Optical Constants of the Noble Metals. *Phys. Rev. B* **1972**, *6*, 4370–4379.
41. Kreibig, U.; Vollmer, M. *Optical Properties of Metal Clusters*, Springer Series in Material Science; Springer: Berlin, 1995; Vol. 25.
42. Fofang, N. T.; Grady, N. K.; Fan, Z.; Govorov, A. O.; Halas, N. J. Plexciton Dynamics: Exciton-Plasmon Coupling in a J-Aggregate-Au Nanoshell Complex Provides a Mechanism for Nonlinearity. *Nano Lett.* **2011**, *11*, 1556–1560.
43. Ashkin, A.; Dziedzic, J. M.; Bjorkholm, J. E.; Chu, S. Observation of a Single-Beam Gradient Force Optical Trap for Dielectric Particles. *Opt. Lett.* **1986**, *11*, 288–290.
44. Maragò, O. M.; Bonaccorso, F.; Saija, R.; Privitera, G.; Gucciardi, P. G.; Iatì, M. A.; Calogero, G.; Jones, P. H.; Borghese, F.; Denti, P.; *et al.* Brownian Motion of Graphene. *ACS Nano* **2010**, *4*, 7515–7523.
45. Maragó, O. M.; Jones, P. H.; Bonaccorso, F.; Scardaci, V.; Gucciardi, P. G.; Rozhin, A.; Ferrari, A. C. Femtonewton Force Sensing with Optically Trapped Nanotubes. *Nano Lett.* **2008**, *8*, 3211–3216.
46. Jauffred, L.; Richardson, A. C.; Oddershede, L. B. Three-Dimensional Optical Control of Individual Quantum Dots. *Nano Lett.* **2008**, *8*, 3376–3380.
47. Messina, E.; Cavallaro, E.; Cacciola, A.; Iatì, M. A.; Gucciardi, P. G.; Borghese, F.; Denti, P.; Saija, R.; Compagnini, G.; Meneghetti, M.; *et al.* Plasmon-Enhanced Optical Trapping of Gold Nanoaggregates with Selected Optical Properties. *ACS Nano* **2011**, *5*, 905–913.
48. Kane, B. E. Levitated Spinning Graphene Flakes in an Electric Quadrupole Ion Trap. *Phys. Rev. B* **2010**, *82*, 115441.
49. Li, T.; Kheifets, S.; Medellin, D.; Raizen, M. G. Measurement of the Instantaneous Velocity of a Brownian Particle. *Science* **2010**, *328*, 1673–1675.
50. Epstein, P. S. On the Resistence Experienced by Spheres in Their Motion through Gases. *Phys. Rev.* **1924**, *23*, 710–733.
51. Barker, P. F. Doppler Cooling a Microsphere. *Phys. Rev. Lett.* **2010**, *105*, 073002.
52. Borghese, F.; Denti, P.; Saija, R.; Iatì, M. A. Optical Trapping of Nonspherical Particles in the T-Matrix Formalism. *Opt. Express* **2007**, *15*, 11984–11998.
53. Saija, R.; Denti, P.; Borghese, F.; Maragó, O. M.; Iatì, M. A. Optical Trapping Calculations for Metal Nanoparticles. Comparison with Experimental Data for Au and Ag Spheres. *Opt. Express* **2009**, *17*, 10231–10241.

54. Saija, R.; Iatì, M. A.; Giusto, A.; Denti, P.; Borghese, F. Transverse Components of the Radiation Force on Nonspherical Particles in the T-Matrix Formalism. *J. Quant. Spectrosc. Radiat. Transfer* **2005**, *94*, 163–179.
55. Klačka, J.; Kocifaj, M. Motion of Nonspherical Dust Particle under the Action of Electromagnetic Radiation. *J. Quant. Spectrosc. Radiat. Transfer* **2001**, *70*, 595–610.